Progress In Electromagnetics Research M, Vol. 102, 233–241, 2021

MIMO Antenna Phase Error Effects on Capacity

Chengyi Chu and Nicholas E. Buris*

Abstract—This paper describes the ramifications in the capacity of Multiple Input Multiple Output(MIMO) wireless links when the antenna systems involved are mischaracterized and contain phase errors. Errors in simulated as well as measured radiation patterns are considered. Also, simple deterministic Line of Sight and stochastic propagation environments are examined. The analyses are carried out on a 2×2 MIMO system. Results show that the resultant error in capacity depends on the degree of the phase error between the antenna ports, the type of propagation environment, as well as the degree of the illumination Signal to Noise Ratio (i-SNR).

1. INTRODUCTION

Measured and simulated radiation patterns of Multi Element Antenna (MEA) systems suffer from a certain degree of phase errors. For example, the quiet zone of a typical anechoic chamber is not illuminated by a single plane wave during a test. The reflections from the walls cause phase errors which is manifested via a free space interference pattern which can be characterized by measuring the field strength with a probe as it crosses the quiet zone along any direction of interest. Furthermore, MEAs, by definition, have several elements, each driven by its own port. When the MEA is placed in the quiet zone of an anechoic chamber for testing, it is more convenient to rotate the MEA about a point fixed on the structure and measure each port separately without changing the center of rotation. The alternative of placing each individual element of the MEA at the center of rotation is cumbersome, especially for a large number of elements, and prone to errors because of the continual physical movement of the Antenna Under Test (AUT) which could suffer from repeatability errors [2]. However, this approach means that different antenna elements follow different trajectories during testing, and as a result, they are exposed to different parts of the quiet zone. This introduces errors in not just the magnitude, but also the phase of the radiation pattern of each of the elements of the MEA.

In [3], it has been shown that the full characterization of an MEA system for MIMO enabling wireless links requires that the full $N \times N$ S-parameter matrix of the N-port MEA together with its N "active E-field gains", $\overline{g}_n(\theta, \varphi)$, corresponding to each port be measured. In [11], a similar conclusion is made using a set of orthonormal modes instead of the active E-field gain. The active E-field gain is the normalized E-field, both polarizations, in the far field when a port is excited, and all other ports are terminated to some load impedance. Unlike the single port antenna case, the active E-field gain of MEAs depends on the termination impedances. However, impedance transformations exist to represent the active E-field gains of one set of terminations in terms of another [4].

There are some measurement facilities which go to extreme lengths to ensure accuracy in antenna measurements, e.g., [1]. Most antenna measurement facilities and anechoic chambers exhibit typical gain and phase errors. In [10], the accuracy of pattern measurements of MEAs is related to the accuracy of their associated equivalent circuit models. In this paper, we examine the measured and simulated E-field phase error effects on the capacity of a wireless link. To our knowledge, such studies have not

Received 21 January 2021, Accepted 4 June 2021, Scheduled 6 June 2021
* Corresponding author: Nicholas E. Buris (nick.buris@nebens.com).
The authors are with the School of Communication and Information Engineering, Shanghai University, Shanghai 200444, China.

been performed before. We artificially add phase errors to the dually polarized measured and simulated active E-field gains of a 2-port MEA. We then measure and simulate the 2×2 S-parameter matrix of the MEA and introduce this information into a system level analysis of a 2×2 link with the same antenna system on either side of the link. We perform the system analyses for both deterministic Line of Sight (LoS) and the stochastic 3GPP Extended Spatial Model (SCME) propagation models [5]. We then compare the Cumulative Distribution Function (CDF) of the capacity for various levels of introduced error. Additionally, we provide quantitative information on the inherent phase errors of our measurements in an anechoic chamber. The effects of the phase errors are expected to be a function of the smart algorithm used in the transmission mode. In Open Loop (OL), the transmitter does not know the channel. So, a different signal, orthogonal to all others, leaves from each antenna. On the other hand, in closed loop Beamforming (BF), the transmitter knows the channel, and the same signal is transmitted from all antennas. However, each antenna is weighted appropriately in amplitude and phase so as to beamform the signal toward the highest gain direction in the channel.

2. PHASE ERRORS ANALYSIS

2.1. Methodology and the MEA under Test

We consider a 2×2 MIMO wireless link consisting of a typical $\pm 45^\circ$ pair of collocated half-wave dipoles at the Tx and a pair of Ultra Wide Bandwidth (UWB) monopoles at the Rx. We manually add phase errors to the dually polarized active E-field gain of a 2-port MEA. We then simulate and measure the 2×2 S-parameter matrix of the MEA and introduce this information into a system level analysis of a 2×2 link. All analyses and measurements have been done at 4.0 GHz.

Figure 1 shows the UWB 2-port MEA Rx antenna system. It is a planar monopole design where the microstrip extends beyond the ground plane and morphs into the UWB monopole. The active E-fields $\overline{g}_1(\theta, \varphi)$ and $\overline{g}_2(\theta, \varphi)$ of ports 1 and 2 when driven by the voltage sources V_{g1} and V_{g2}, respectively, are combined according to Eq. (1) to produce the total far field of the MEA. Two such instantiations of the far field are shown in Fig. 2 under two different excitations, i.e., port 1 only in Fig. 2(a) and ports 1 and 2 equally excited in Fig. 2(b).

$$\overline{E}(\theta, \varphi) = V_{g1}\, \overline{g}_1(\theta, \varphi) + V_{g2}\, \overline{g}_2(\theta, \varphi) \tag{1}$$

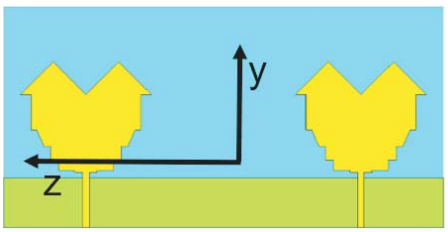

Figure 1. The UWB 2-port MEA system. The "Green" strip represents ground metallization on the bottom side of the pcb. The "yellow" metallization on the top side represents the microstrips and their transition into monopoles.

We next use Eq. (2) to make an artificial addition of a phase error to the simulated active E-field of port 2 of the MEA.

$$\overline{g}_2(\theta, \varphi) \rightarrow \overline{g}'_2(\theta, \varphi) = \overline{g}_2(\theta, \varphi) e^{j\psi(\theta, \varphi)} \tag{2}$$

At each orientation (θ, φ), the function $\psi(\theta, \varphi)$ is an independent uniform random variable in the interval $[-\sigma, \sigma]$ and represents the relative phase error between the active E-fields of ports 1 and 2. The phase error is added only in the simulated results of port 2. Furthermore, this phase error is not to be confused with Channel State Information (CSI) which also results in channel matrix errors and subsequent errors in the system's smart algorithms [6].

We place the Tx and Rx at a fixed distance between them and adjust the Tx power so as to effect a different average Illumination Signal to Noise Ratio (i-SNR) at the Rx antennas. The i-SNR is the

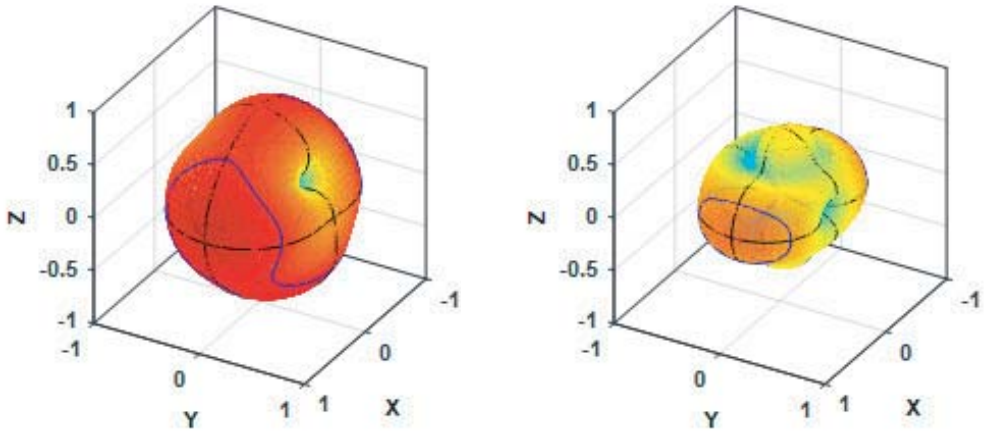

Figure 2. Active E-field gains of two different excitations. (a) $V_{g1} = 1$, $V_{g2} = 0$ and (b) $V_{g1} = V_{g2} = 1$.

SNR experienced by an ideal isotropic radiator, not by the actual Rx, and is used here, as in [2], in order to make a meaningful and fair comparison of the results. Further, we connect Tx and Rx via a propagation model to obtain the channel and, subsequently, the Shannon capacity of the link under Open Loop (OL) and closed loop Beamforming (BF) transmission modes [7, 8]. The channel matrix includes the effects of $50\,\Omega$ termination impedances. Two propagation models have been examined in this work; first a free-space, deterministic, Line of Sight (LoS) and second the 3GPP Extended Spatial Model (SCME) [5]. The SCME is basically a plane wave decomposition of the propagation environment consisting of a total of 120 plane waves bundled in 6 clusters of 20 plane waves each. The specific polarimetric characteristics of these plane waves follow statistics as described in [5]. In the LoS case, we rotate the Rx in 1296 different 3-dimensional orientations. In the SCME, we reduce the number of rotations to 15, but since SCME is inherently random, we also generate 100 random instantiations of the propagation environment for each orientation. This approach yields the statistically robust samples of 1296 and 1500 capacity values for the LoS and the SCME case, respectively. We then compare the Cumulative Distribution Function (CDF) of these capacity samples for various levels of introduced error.

2.2. Capacity Effects of Phase Errors (Simulated Patterns)

The Shannon capacity for OL and BF transmission modes is simulated for the 2×2 MIMO wireless link described above [5]. In our formulation, we have modified the standard channel formulas by incorporating antenna impedance termination effects. All these terminations are assumed to be $50\,\Omega$ here in order to be consistent with the measurements taken by the network analyzer of the anechoic chamber.

The OL and BF capacity CDF are shown in Fig. 3 for various i-SINR, propagation models, and the degree of added uniform random phase error between ports 1 and 2 of the simulated 2-port MEA. There are several methods to calculate mean capacity (e.g., see [9]). However, here, the mean capacity difference result between with and without the phase error is calculated by Equation (3) and tabulated in Table 1 and Table 2.

$$Capacity\Delta = 2\frac{\langle C\rangle_{W/O\_err} - \langle C\rangle_{With\_err}}{\langle C\rangle_{W/O\_err} + \langle C\rangle_{With\_err}} \tag{3}$$

It is seen that, in general, the larger the phase error the larger the capacity difference (see Table 1 and Table 2). Also, the capacity difference in the LoS case is larger than that of the SCME propagation model case. There are two main factors for this. First, the BF capacity is obtained by performing a singular value decomposition of the channel which, as part of the beamforming algorithm, is considered known. So, the phase errors added to the active E-field gain of port 2 are taken into account with the

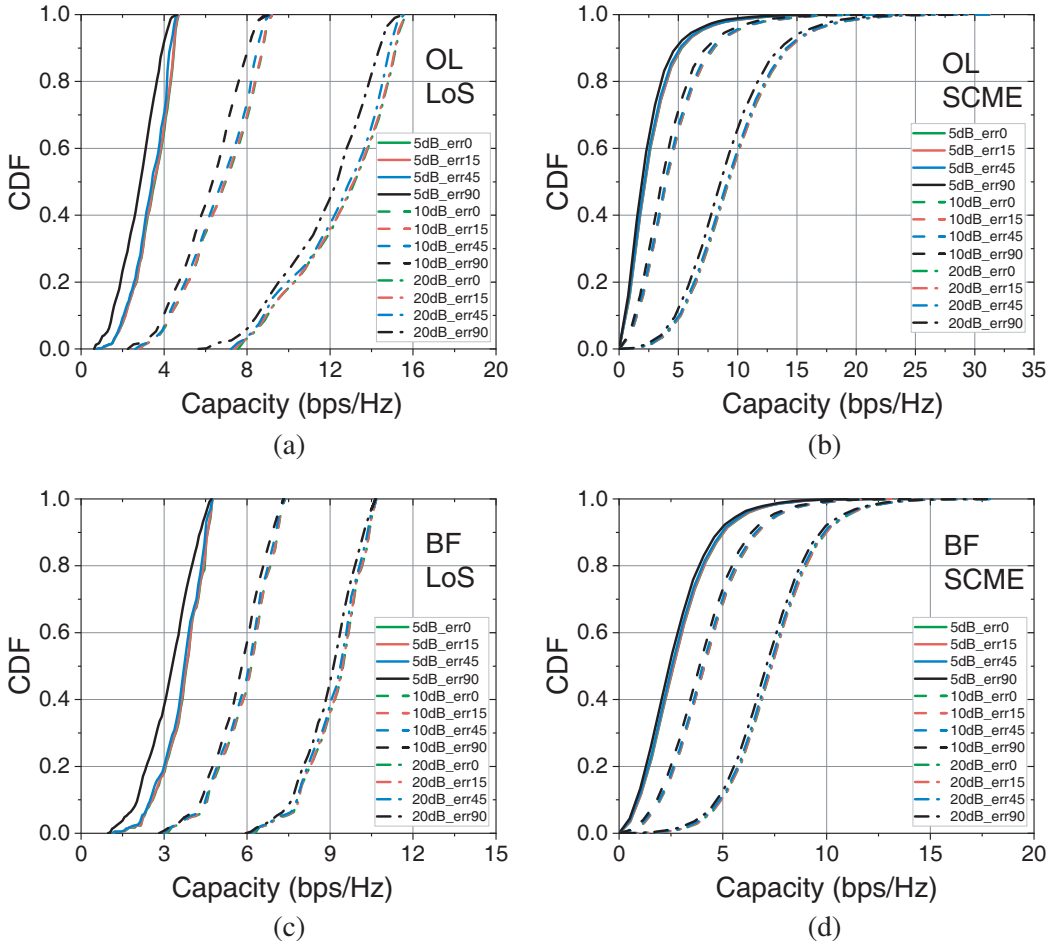

Figure 3. Capacity CDF for different values of i-SINR (i.e., 5 dB, 10 dB, 20 dB) and phase error ($\sigma = 0$ (*no error*), $\sigma = \pm 15°, \pm 45°, \pm 90°$). Simulated active E-field patterns are used. (a) OL and LoS conditions; (b) OL and SCME; (c) Beamforming and LoS; (d) Beamforming and SCME. Frequency $f = 4.0$ GHz.

Table 1. Mean OL capacity difference (SIMS).

Model	Phase error	5 dB	10 dB	20 dB
LoS	±15°	1.13%	0.72%	0.61%
	±45°	4.02%	2.62%	1.91%
	±90°	17.53%	9.65%	7.75%
SCME	±15°	0.45%	0.41%	0.32%
	±45°	3.21%	2.26%	1.31%
	±90°	12.94%	9.45%	7.47%

channel at the Tx. Second, the recipe for the SCME propagation model involves random variables for, among other parameters, the phase of the E-field pattern [5]. Therefore, adding an artificial phase error as in Eq. (2) does not materially change the physics of the problem. Also, because the capacity increases with the i-SINR, the higher the i-SINR is, the smaller the percentage difference is in the capacity for a fixed level of phase error.

Table 2. Mean BF capacity difference (SIMS).

Model	Phase error	5 dB	10 dB	20 dB
LoS	±15°	0.52%	0.48%	0.21%
	±45°	2.69%	2.38%	1.12%
	±90°	14.91%	7.12%	3.66%
SCME	±15°	0.38%	0.24%	0.14%
	±45°	2.38%	1.47%	1.06%
	±90°	8.31%	5.85%	3.49%

2.3. Capacity Effects of Phase Errors (Measured Patterns)

In Appendix A, we describe the errors in the phase of the E-fields measured in an anechoic chamber. The source of the errors is the reflected waves in the quiet zone and the fact that, for 3-D measurements, the antennas are rotating about a point and are found at different points in the quiet zone for each (θ, φ) orientation. In this section, we repeat the above methodology, but instead of artificially adding a phase error to the simulated fields of one port (see Eq. (2)), we simply add the phase errors to the

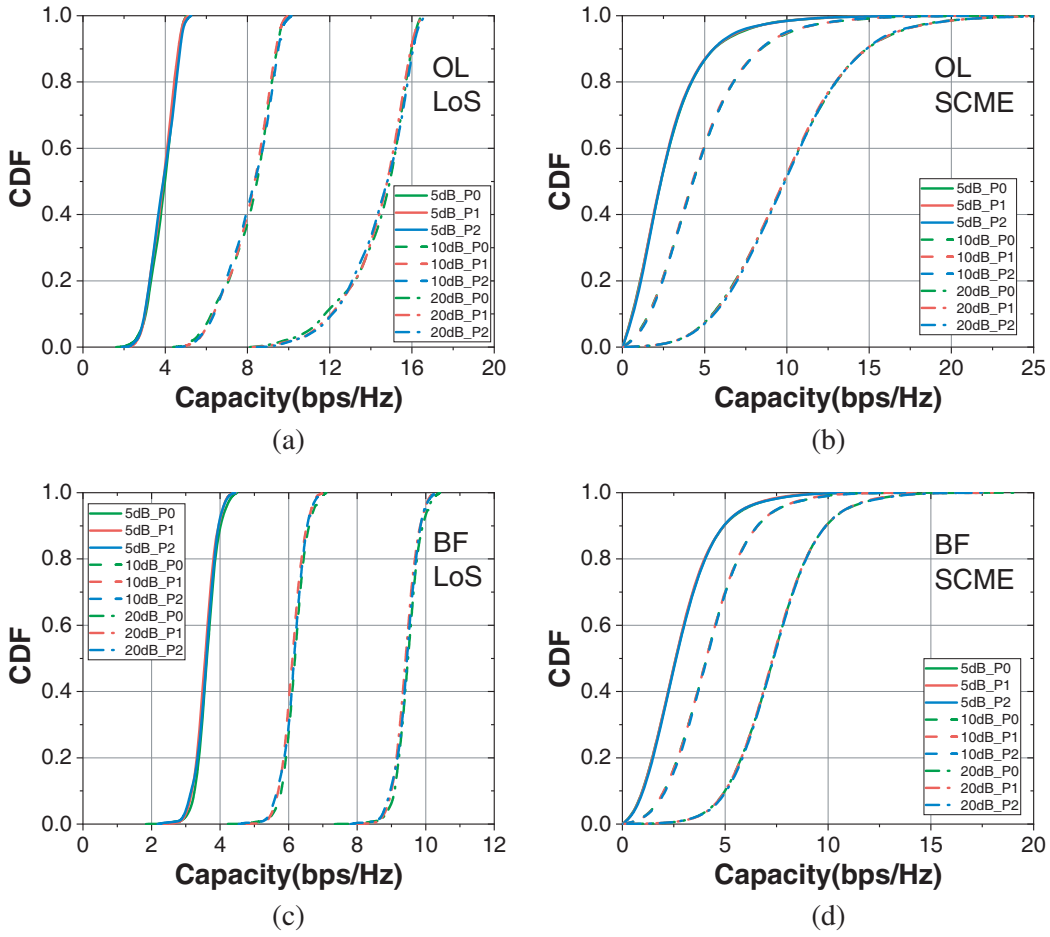

Figure 4. Capacity CDF for different values of i-SINR (i.e., 5 dB, 10 dB, 20 dB) and antenna placement (P0, P1 and P2) in the quiet zone. Measured patterns with their inherent phase errors are used. (a) OL and LoS; (b) OL and SCME; (c) Beamforming and LoS; (d) Beamforming and SCME. Frequency $f = 4.0$ GHz.

measured active E-field patterns.

The capacity effects of the phase errors are expected to be a function of the smart algorithm used in the transmission mode. In Open Loop (OL) the transmitter does not know the channel. So, a different signal, orthogonal to all others, leaves from each antenna [7]. In closed loop Beamforming (BF), the transmitter knows the channel, and the same signal is transmitted from all antennas. However, each antenna is weighted appropriately in amplitude and phase so as to beamform the signal toward the highest gain direction in the channel [8].

In Fig. 4, we show the OL and BF capacity CDF resulting from the measured 2-port MEA patterns for different i-SINR levels, propagation models, and 3 positions in the quiet zone along the Tx-Rx axis. We use a formula like Eq. (3) to construct Table 3 and compare the mean capacity difference between the best and worst performances for different test (measured) positions along the Tx-Rx axis.

Table 3. Mean capacity difference (MEAS).

Model	Phase error	5 dB	10 dB	20 dB
LoS	OL	2.03%	1.53%	0.81%
	BF	1.67%	1.13%	0.74%
SCME	OL	1.28%	1.16%	0.76%
	BF	1.13%	0.98%	0.61%

From Fig. 4, it can be seen that the variations in the capacity because of the expected different phase errors at different points in the quiet zone are relatively negligible. This is because these phase errors are random, and they apply equally to both antenna elements. Furthermore, the magnitude of the measured patterns is almost independent of the position in the quiet zone. Therefore, the phase difference between the two antenna patterns at a given (θ, φ) orientation does not change appreciably from point to point in the quiet zone.

3. CONCLUSIONS

In this paper, we examine the effect of relative phase errors between the ports of a 2-port MEA when it comes to the resultant Shannon capacity. We find that the capacity errors are a function of the degree of the phase errors. They are higher for deterministic propagation models as opposed to randomness based 3GPP models, and they become relatively less important with higher i-SINR values. Additionally, the beamforming algorithm is a little more forgiving of such phase errors than the open loop transmission mode. It is important to evaluate MEAs in terms of their capacity performance. This work, especially when being extended with more propagation models, could lead to mappings of threshold antenna pattern phase errors to minimum tolerable capacity performance errors and uncertainty.

APPENDIX A. PHASE ERROR CHARACTERIZATION

In order to represent the phase measurement errors in the quiet zone of our chamber, we perform the following test. As shown in Fig. A1, we perform 3-D vector measurements of both polarizations of E-field of the 2-port MEA. We then parallel-displace the MEA by a vector $\bar{d}$ to a different position in the quiet zone and measure the patterns again. For small d, these two measured patterns should be related by a simple phase difference, $\psi = kd \cdot cos(\bar{r}, \bar{d})$, where $\bar{r} = (\sin\theta\cos\varphi, \sin\theta\sin\varphi, \cos\theta)^t$ and k is the wave number. Finally, we process the measured data and form the ratio:

$$kd = \frac{\psi}{\cos(\bar{r}, \bar{d})} \tag{A1}$$

Under a single plane wave illumination, this kd should be constant on the entire 4π sphere. Deviations from a constant represent phase errors in the measurements due to the presence of reflections in the quiet zone.

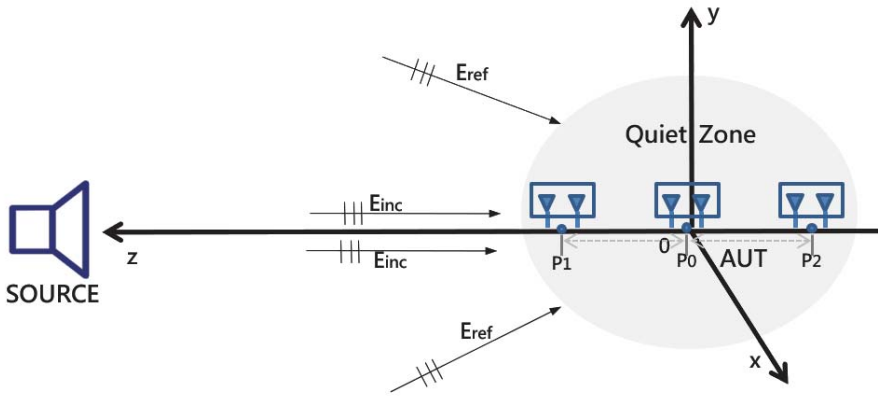

Figure A1. The coordinate system used in the chamber measurements.

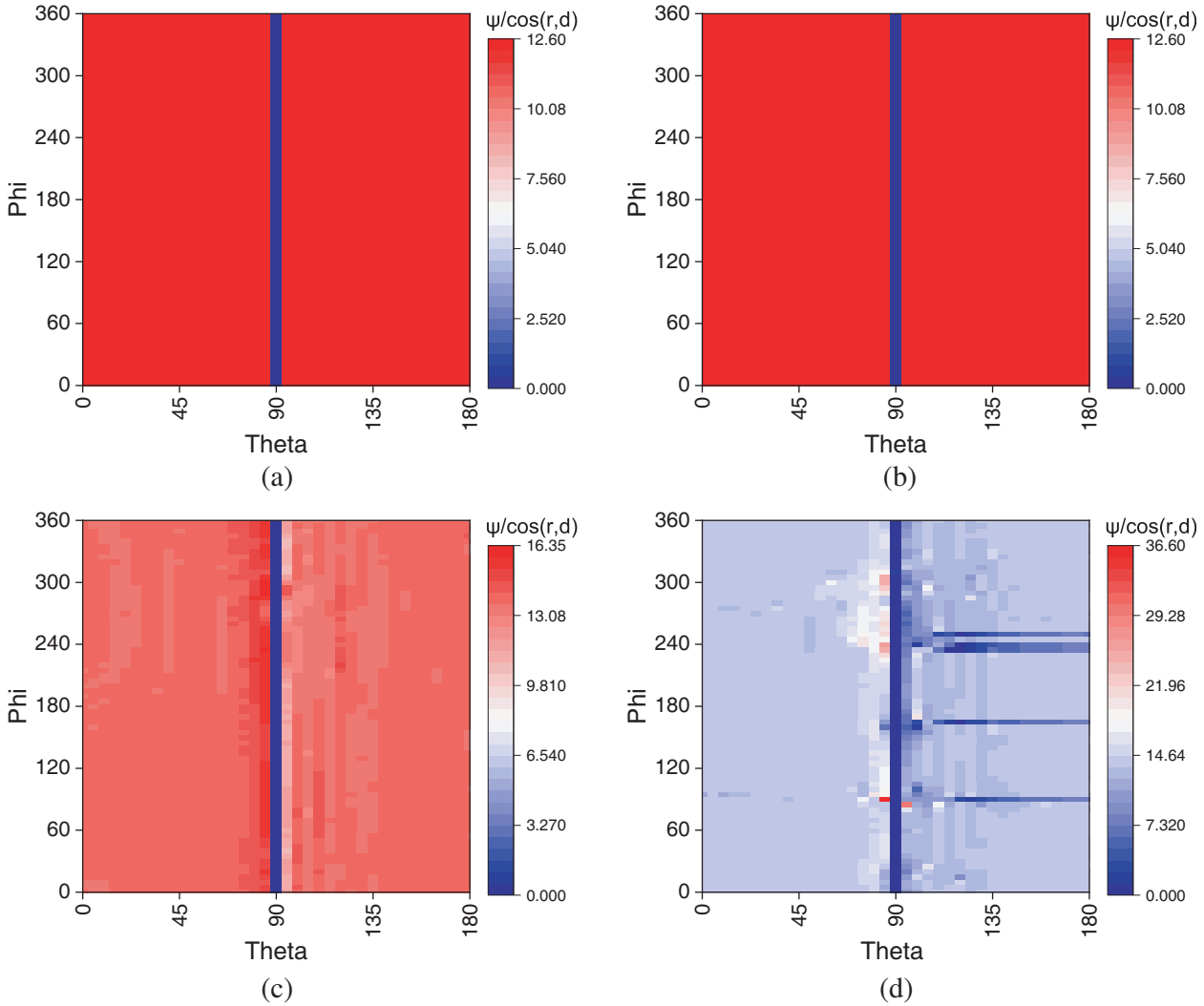

Figure A2. The value of the "constant" "kd" parameter over the full sphere (i.e., $\theta \in [0, 180°]$ and $\varphi \in [0, 360°]$). (a) Simulated E_θ pattern. (b) Simulated E_φ pattern. (c) Measured E_θ pattern. (d) Measured E_φ pattern.

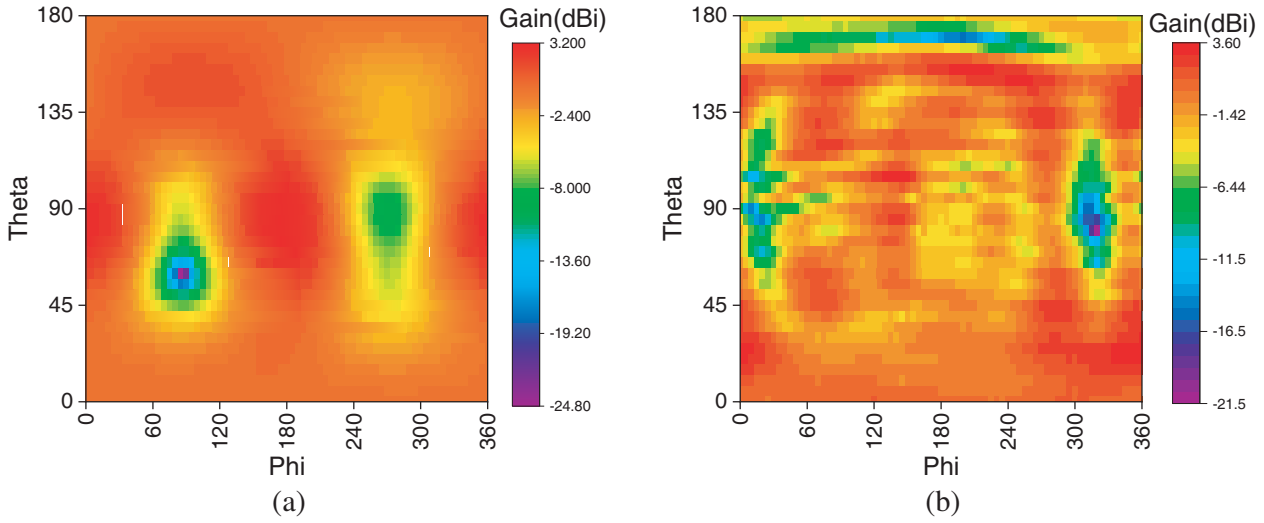

Figure A3. Radiation pattern (power gain) simulations vs. measurements. (a) Simulated port 1 radiation pattern. (b) Measured port 1 radiation pattern.

Figure A2 shows constant kd over the sphere for the simulated and measured patterns of the 2-port MEA. When $\theta = 90°$, the two monopoles are symmetrically located with respect to the z-axis (see Fig. A1). Therefore, $\cos(\bar{r}, \bar{d})$ is zero as manifested by the "blue" line in Fig. A1. The simulated patterns obey the constancy of kd inherently which reflects the numerical consistency of the electromagnetic solver used here (i.e., CST MWS). The measured patterns show the phase errors which are significantly higher at some points in the E_φ polarization. But in most parts of measured patterns of E_θ and E_φ polarizations, the calculation result fluctuates around and close to this constant. Expectedly, the magnitudes of the measured and simulated patterns differ, as can be seen in Fig. A3. The magnitude of the patterns measured at different points in the quiet zone of our chamber are essentially identical.

REFERENCES

1. Gordon, J. A., D. R. Novotny, M. H. Francis, R. C. Wittmann, M. L. Butler, A. E. Curtin, and J. R. Guerrieri, "Millimeter-wave near-field measurements using coordinated robotics," *IEEE Transactions on Antennas and Propagation*, Vol. 63, No. 12, 5351–5362, 2015.
2. CTIA, "Test plan for 2 × 2 downlink MIMO and transmit diversity over-the-air performance," Sep. 2017.
3. Buris, N. E., "Active E-field gain: Toward a standard description of MEAs," *IEEE International Symposium on Antennas and Propagation & USNC/URSI National Radio Science Meeting*, 2061–2062, 2017.
4. Buris, N. E., "Antenna termination transformations in MoM," *IEEE Antennas & Propagation Symposium*, 967–968, San Diego, CA, 2017.
5. Baum, D., J. Hansen, J. Salo, G. Del Gadldo, M. Milojevic and P. Kyosti, "An interim channel model for beyond-3G systems: Extending the 3GPP Spatial Channel Model (SCM)," *Vehicular Technology Conference*, Stockholm, 2005.
6. Thian, B. S., H. D. Nguyen, and S. Sun, "Statistical precoding for MIMO systems with channel estimation errors," *IEEE Wireless Communications Letters*, Vol. 4, No. 1, 62–65, 2014.
7. Foschini, G. and M. Gans, "On limits of wireless communications in a fading environment when using multiple antennas," *Wireless Personal Communications*, Vol. 6, 311–335, 1998.
8. Goldsmith, A., *Wireless Communications*, Cambridge University Press, 2005.
9. Varzakas, P., "Average channel capacity for rayleigh fading spread spectrum MIMO systems," *International Journal of Communication Systems*, Vol. 19, No. 10, 1081–1087, Dec. 2006.

10. Wallace, J. W. and R. Mehmood, "On the accuracy of equivalent circuit models for multi-antenna systems," *IEEE Transactions on Antennas and Propagation*, Vol. 60, No. 2, 540–547, 2012.
11. Lynch, J. J., "A modal description of multiport antennas," *International Journal of Antennas and Propagation*, Vol. 2011, Article ID 438437, doi:10.1155/2011/438437.